

Effect of the mechano-chemical activation, pressing and sintering the powders of 70% Fe, 30% BaTiO₃ on morphology, microstructure, magnetic and electrical properties

M. PLAZINIC^a, M. SPASOJEVIC^{b,*}, M. LUKOVIC^a, A. MARICIC^a, M. D. SPASOJEVIC^a

^aJoint Laboratory for Advanced Materials of SASA, Section for Amorphous Systems, Faculty of Technical Sciences, Čačak, University of Kragujevac, Čačak, Serbia

^bInnovation Center of the Faculty of Chemistry, University of Belgrade, Belgrade, Serbia

The effect of grinding time of a powder mixture of 70wt% Fe and 30wt% BaTiO₃ on properties of as-obtained and sintered powders is studied. The composition, phase structure, morphology, magnetic and electrical properties depend on the grinding time. The powder, ground for 150 min shows the highest magnetization. Compact samples, in which the BaFe₁₂O₁₉ crystals of optimal sizes form completely, are obtained by sintering the pressed powder, ground for 240 min, at 1200°C. These samples show the highest magnetization and dielectric permittivity. Annealing of sintered samples at Curie temperatures results in the structural relaxation. Samples cooled in magnetic field show 1.96 higher magnetization than as sintered.

(Received August 21, 2020; accepted August 16, 2021)

Keywords: Milling, Sintering, Microstructure, Magnetic properties, Electrical properties, Magnetization, Dielectric permittivity

1. Introduction

Multiferroic materials exhibiting both electric and magnetic polarization, have been examined by many research groups in recent years due to their potential technological applications in various microelectronic devices, including microwave phase shifters, magnetically controlled electro-optic devices and broadband magnetic field sensors [1–5]. Barium hexaferrites, BaFe₁₂O₁₉ have high corrosion and wear stability, high uniaxial magnetic anisotropy, high coercivity and low production cost [6–8]. Several BaFe₁₂O₁₉ preparation procedures, such as co-precipitation, sol-gel combustion, micro-emulsion and ball millings, have been developed [9–13]. The synthesis route of BaFe₁₂O₁₉ determines its microstructure, morphology, electrical and magnetic properties [6–23]. Lately, a ball milling processing has been a promising technique for producing a wide range of nanostructures and magnetic materials [12, 13, 21–26]. Grinding of precursors results in formation of fine particles with a large contact surface and a high density of dislocations on the surface. An increase in these contact surfaces, reduction of the particle size and the storage of strain energy in particles are of the greatest importance in increasing the rate of BaFe₁₂O₁₉ formation [24]. Therefore, the grinding time substantially affects time and temperature of sintering [12, 13, 21, 22, 24–26]. Also, the grinding time determines the morphology and microstructure of the obtained powders and thus, their electrical and magnetic properties. [12, 13, 21, 22, 24–26]. A study of dielectric and magnetic properties of mechanochemically prepared barium hexaferrite has shown improved magnetic properties with increasing the grinding

time whereas the electric permittivity has shown a small change [12, 13].

The aim of this study is to prepare the active mixture with fine particles by grinding the powders consisting of 70 wt% Fe and 30 wt% BaTiO₃ and furthermore, barium hexaferrite by sintering this active mixture. Also, the effect of the grinding time and annealing temperature on morphology, microstructure, magnetic and electrical properties of the obtained samples was investigated.

2. Experimental

Powders Fe (Aldrich, St. Louis, MO, p.a. 99.99 wt%) and BaTiO₃ (Aldrich, St. Louis, MO, p.a. 99 wt%) were mixed in 70:30 wt ratio and ground in a planetary ball mill (Retsch PM 400) in air. The grinding time of the powder was from 30 to 360 min. Powders were pressed under the pressure of 500 MPa into disk shape samples, with diameter of 8 mm and thickness of 1.5 mm. They were sintered in air in a laboratory chamber furnace (Electron) at 1200°C for 2 h.

The X-ray diffraction patterns of samples were obtained using a Bruker DM X-ray diffraction (XRD) instrument in Bragg-Brentano geometry with a grazing incidence angle of 0.5° using CuK_{α,1} ($\lambda_{K\alpha,1} = 0.15405929$ nm) and CuK_{α,2} ($\lambda_{K\alpha,2} = 0.15444274$ nm) radiation. Diffraction data were acquired over the scattering angle 2θ from 10° to 90° with step of 0.05°. The texture of individual crystalline phases, was obtained using the equation [27]:

$$T_x = i(n^{-1} \sum i_i)^{-1} \quad (1)$$

where: T_x – texture coefficient, i – intensity of an individual reflection belonging to a particular crystal plane normalized against the intensity of that same reflection in a reference sample, and n – total number of reflections of individual crystalline phase considered.

The morphology was analyzed using a Scanning Electron Microscope (SEM, JSM-6390 LV JEOL., 30kV) coupled with EDS. The particle size of samples was determined by a Leica Q500MC automatic device for microstructural analysis. Magnetic measurements were performed by a modified Faraday method based on the effect of an inhomogeneous magnetic field on the powder. Magnetic force measurements were carried out with a sensitivity of 10^{-7} N under argon atmosphere.

The relative dielectric permittivity of samples was measured on a disc using low-frequency impedance

analyzer HP 4119A and high-frequency impedance analyzer HP 4191A. The real and the imaginary part of impedance were measured using measuring mode of parallel RC circuit.

3. Results and discussion

The powder mixture consisting of 70 wt% Fe and 30 wt% BaTiO₃ is ground in a planetary ball mill for different periods of time (from 30 to 360 min). The XRD analysis is used to determine the phase structure of the initial mixture and as-ground powders. XRD patterns of both the initial mixture and as-ground powders show the presence of peaks corresponding to Fe and BaTiO₃. With increasing the grinding time, the size of these peaks decreases, whereas the width at their half height increases [13, 22] (Fig. 1).

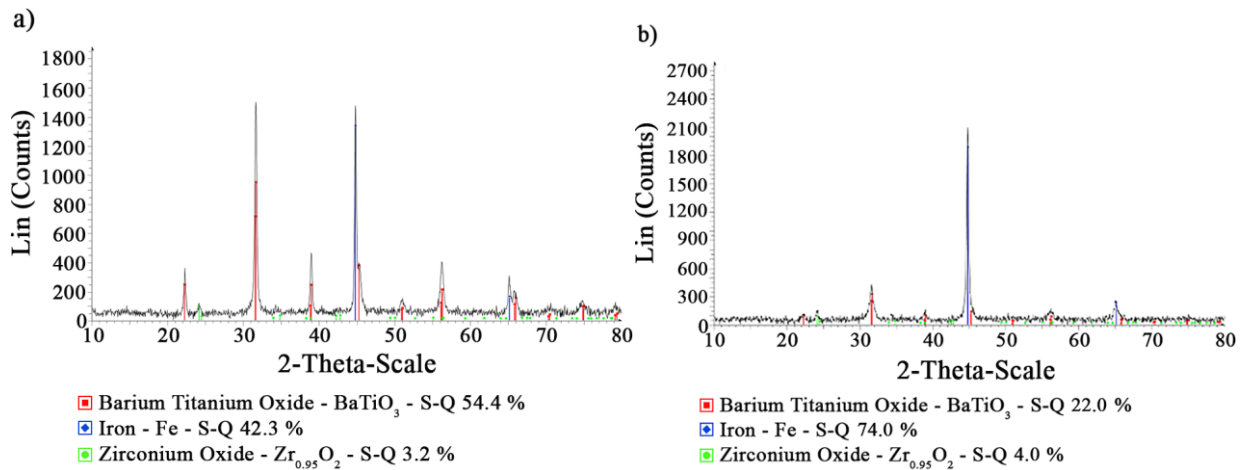


Fig. 1. The XRD - patterns of the samples ground for a) 60 min, b) 240 min (color online)

These results indicate that grinding crushes the crystals of both Fe and BaTiO₃ and increases their inner microstrains (Fig 2, Fig 3).

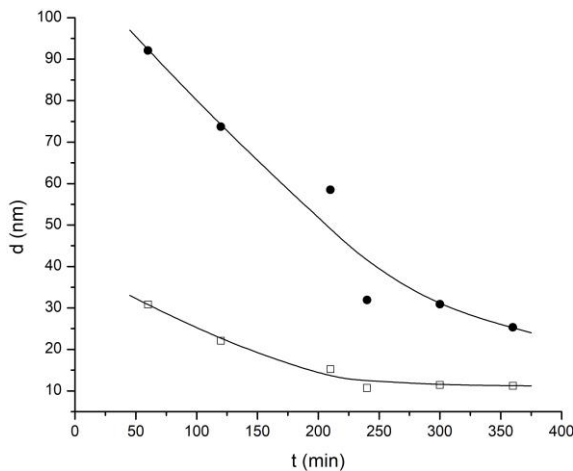


Fig. 2. Dependence of the mean crystalline size on the grinding time: ● - Fe; □ - BaTiO₃.

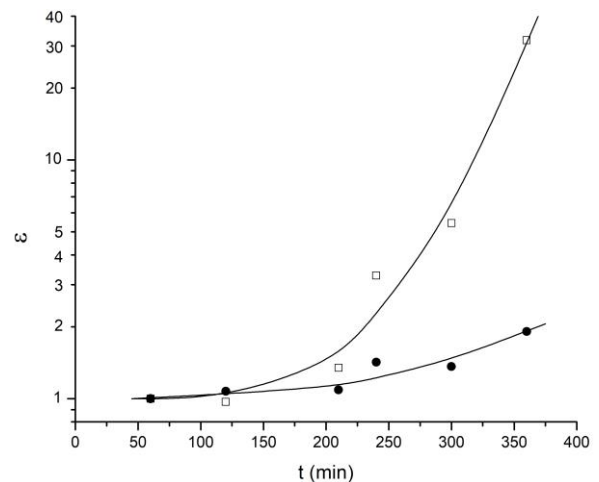


Fig. 3. Dependence of inner microstrains, ϵ , on the grinding time: ● - Fe; □ - BaTiO₃

The intensity of all BaTiO₃ peaks is decreasing proportionally with increasing the grinding time. The same behavior is observed with Fe. This indicates that crushing of Fe and BaTiO₃ crystals does not alter their texture. Values of the texture coefficient of individual crystalline planes are determined using the equation (1). The obtained results show that these values do not depend on the grinding

time. With increasing the grinding time, new, weakly defined peaks of the iron oxides, FeO, magnetite, Fe₃O₄ and hematite, α -Fe₂O₃ are emerging (Fig. 1) [13, 22].

During grinding, mechanical forces cause defects in the crystalline structure of the powder particles. This is especially pronounced in the surface layer of the powder particles. As a result of the thermal energy effect, a local heating of the surface layer of the powder particles occurs. In this case, the increased temperature and the elevated number of dislocations facilitate iron oxidation with air oxygen. A mixture of oxides with the amorphous structure is formed by oxidation. This is confirmed by the EDS analysis, which shows that the increased grinding time causes the elevated content of oxygen in a sample. Longer grinding results in formation of fine nanocrystals of FeO, Fe₃O₄ and α -Fe₂O₃ [13, 22]. The mechanical force and thermal energy also deteriorate the crystalline structure of the surface layer of BaTiO₃ particles and thus, create its amorphous phase. Crushing of the powder particles into smaller by grinding accelerates the process of formation of the BaTiO₃ amorphous phase. Ratios of sum of integrals of peak intensities of the crystalline phase of ground samples to sum of integrals of peaks intensities of the crystalline phase of non-ground samples for Fe and BaTiO₃ are determined. These ratios are used to calculate fractions of the crystalline phases of Fe and BaTiO₃ in the crystalline mixture of the ground sample. By analyzing these integrals we discover that iron is oxidized relatively fast and forms the amorphous phase of oxides when ground for 60 min. Ratio of the rate of Fe oxidation to the rate of amorphization of BaTiO₃ determines the phase content of the ground powder. Based on the obtained values of integrals,

dependence of the weight percentages of the crystalline phase of both Fe and BaTiO₃ in their crystalline mixture on the grinding time is determined (Fig. 4).

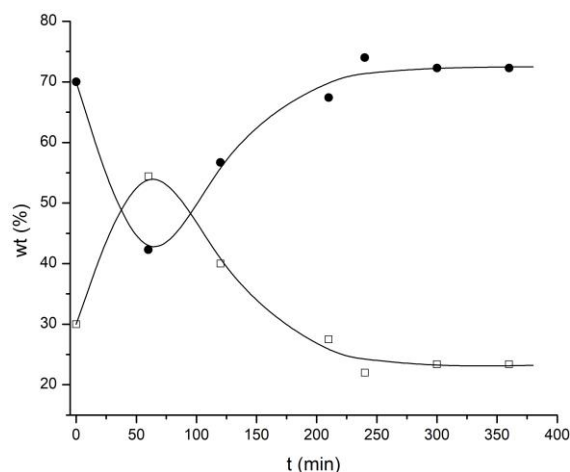


Fig. 4. The weight percentages of the crystalline phases of Fe and BaTiO₃ in their crystalline mixture as a function of the grinding time: ● - Fe; □ - BaTiO₃

SEM micrographs show that morphology of powders depends on the grinding time. Fig. 5 represents the SEM micrographs of a mixture of BaTiO₃ and Fe powders ground for 100 minutes. As seen in Fig. 5, the powder mainly consists of the spherical particles with the mean size of 150 nm. Moreover, particles twinned in a larger particle are found. The particles form agglomerates with the average size of around 2.5 μ m as seen in Fig. 5.b.

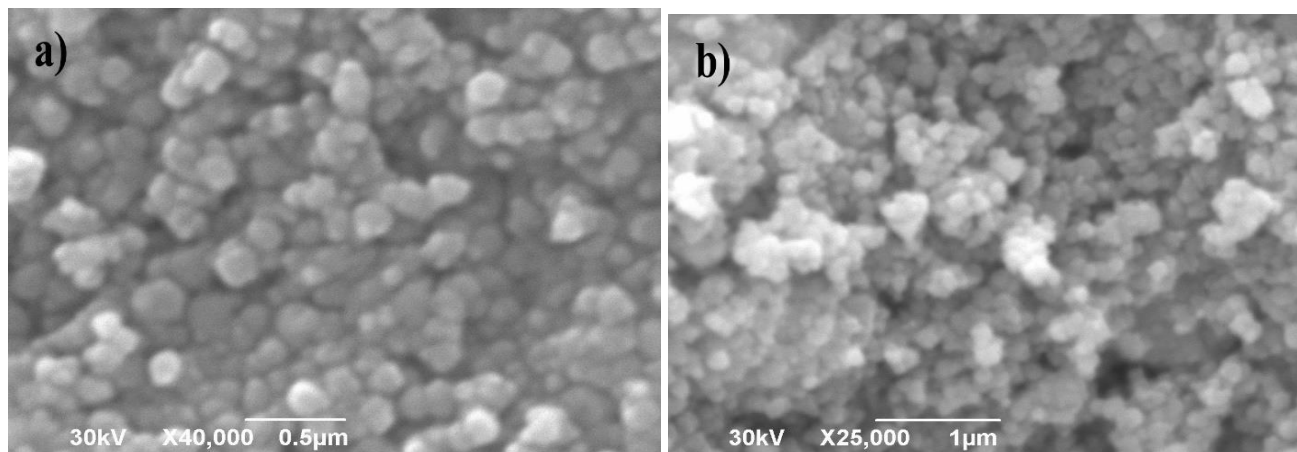


Fig. 5. SEM images of mixture of 70 wt% Fe and 30 wt% BaTiO₃ ground for 100 min

Mapping of the elements of the Fe+BaTiO₃ sample confirms that the sample, ground for 100 minutes, consists

of the mixture of BaTiO₃ and Fe particles and their oxides (Fig. 6).

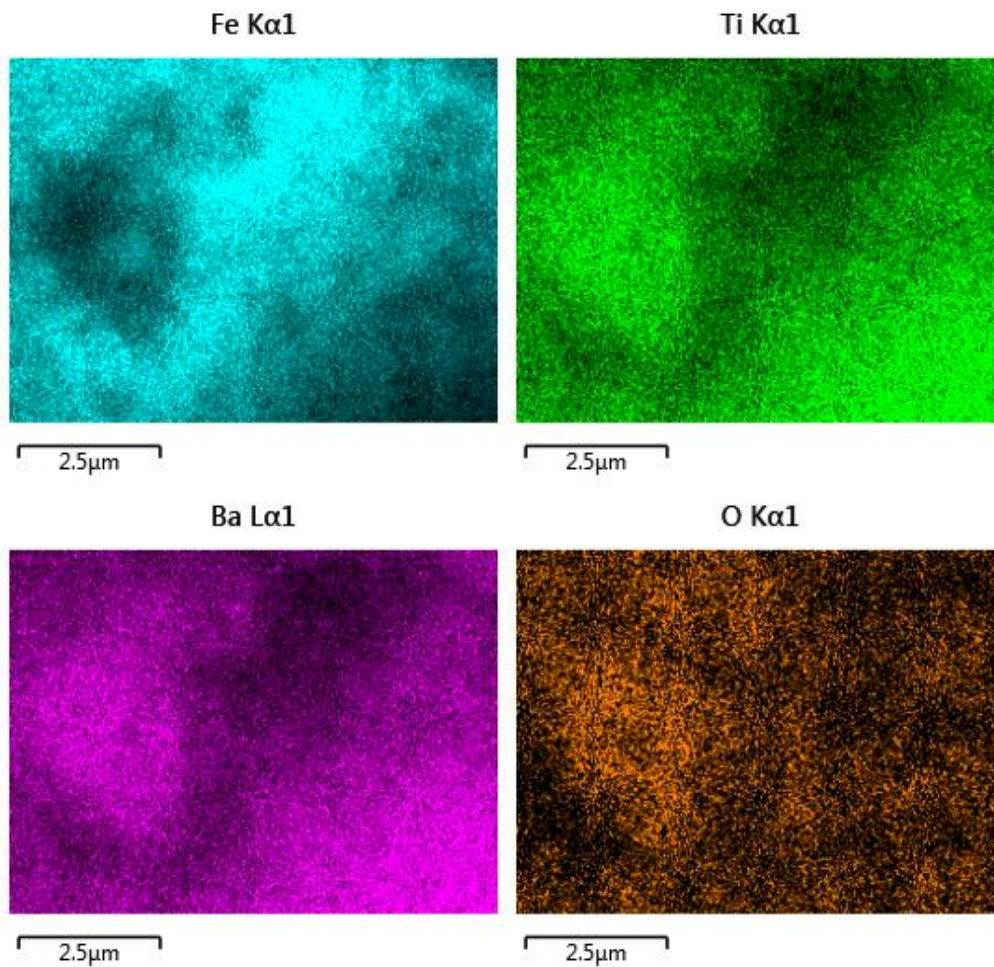


Fig. 6. Chemical mapping of the sample consisting of 70 wt% Fe and 30 wt% BaTiO₃ ground for 100 min (color online)

Besides spherical particles, both polygonal and needle-shaped particles emerge 120 min after the grinding (Fig. 7.).

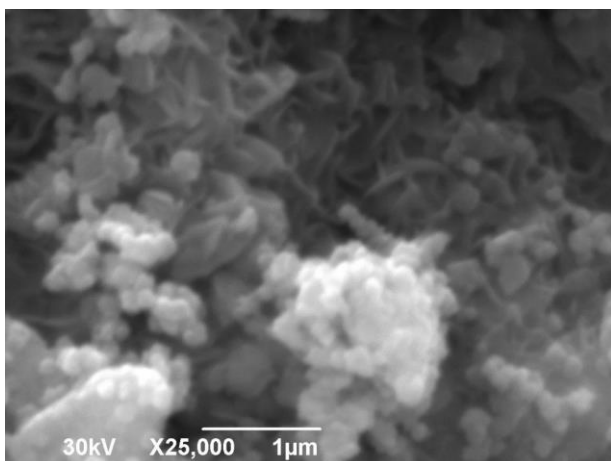


Fig. 7. SEM image of mixture consisting of 70 wt% Fe and 30 wt% BaTiO₃ ground for 120 min

The micrograph of the sample consisting of 70 wt% Fe and 30 wt% BaTiO₃, ground for 150 min (Fig. 8.), shows the presence of not only the spherical particles, but also particles of platelet structures of FeO and Fe-containing

particles of the polygon shape. Mapping of the elements of the Fe+BaTiO₃ sample indicates that the sample, ground for 150 min, consists of agglomerates of BaTiO₃ with the mean size of 10 μm and agglomerates of the Fe-containing particles, whose mean size was about 900 nm.

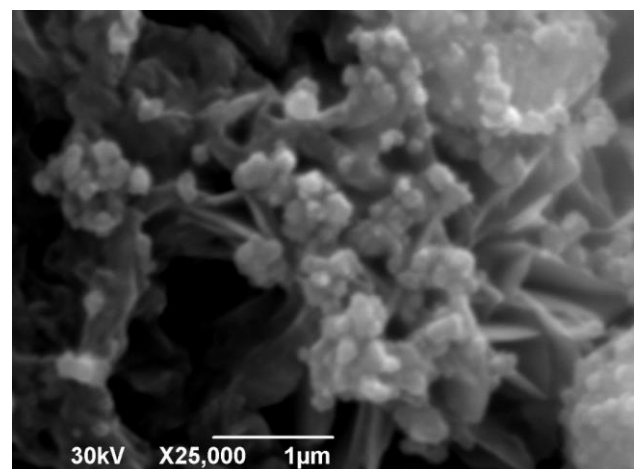


Fig. 8. SEM image of the mixture consisting of 70 wt% Fe and 30 wt% BaTiO₃, ground for 150 min

A SEM image of a sample, ground for 180 minute show that the powder is mainly composed of aggregates of the

polyhedron shape, consisting of spherical particles (Fig. 9). Mapping of the elements allows for determination of the powder composition. The powder is composed of a mixture of BaTiO₃ agglomerates with mean size of about 8 μm and agglomerates of Fe-containing particles whose mean size was 700 nm.

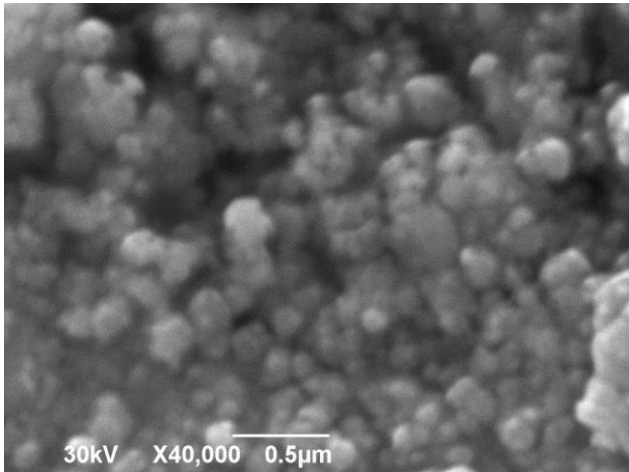


Fig. 9. SEM image of the mixture consisting of 70 wt% Fe and 30 wt% BaTiO₃, ground for 180 min.

The powders obtained after grinding for 210 and 240 min, are composed of agglomerates of various shapes with the mean size of 0.7 and 0.5 μm, respectively, assembled of spherical particles (Fig. 10).

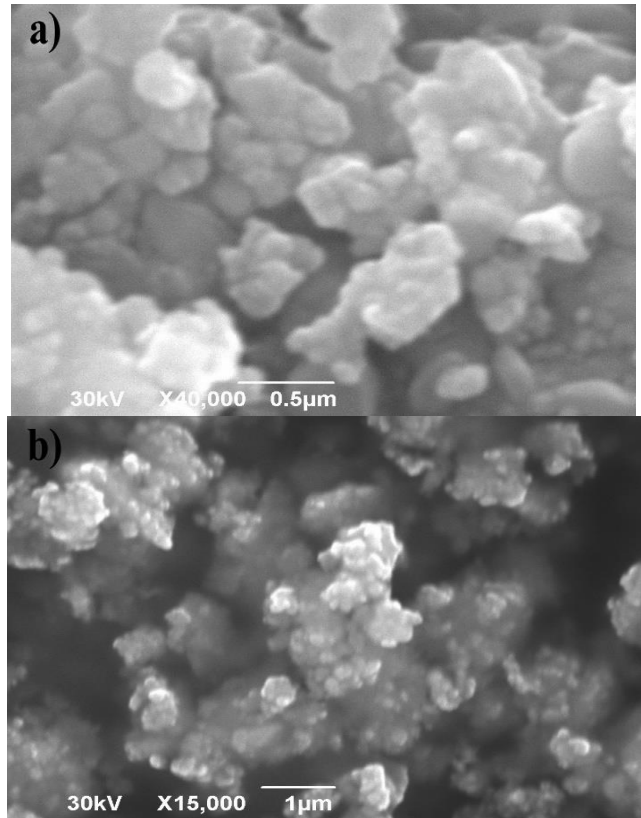


Fig. 10. SEM images of the mixture consisting of 70 wt% Fe and 30 wt% BaTiO₃, ground for a) 210 min and b) 240 min

SEM images, chemical mapping and EDS spectra show that increase in the grinding time results in a) the increase in the mean size of aggregates, reaching the maximum in 150 min. Further increase in the grinding time from 150 to 240 min causes the decrease in the mean size of aggregates; b) the decrease in the mean size of spherical particles and c) the increase in the oxygen content in the powder (Fig. 11) [22].

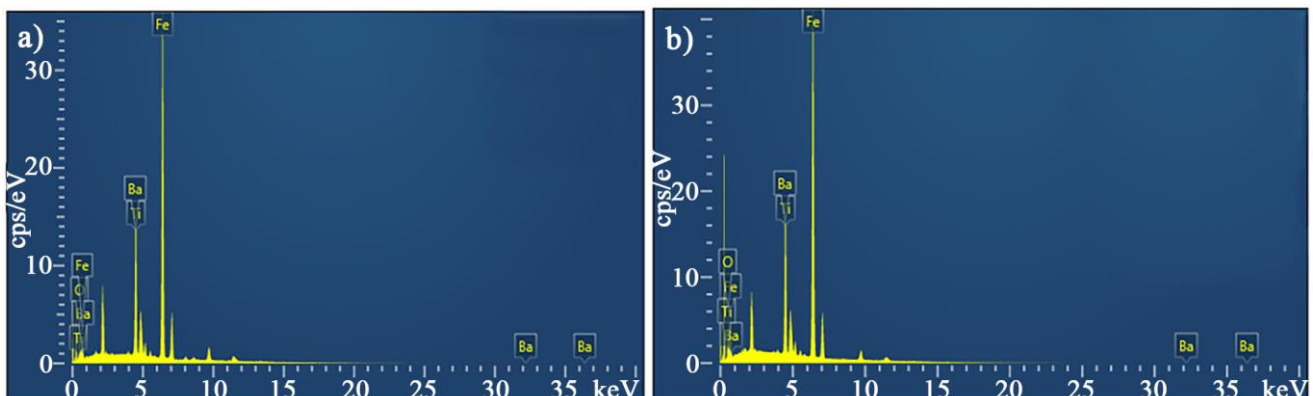


Fig. 11. EDS spectra of samples ground for: a) 120 min and b) 240 min (color online)

SEM images of powders sintered at 1200°C show that the grinding time substantially affects the efficiency of the sintering process (Fig. 12) [13]. During sintering, a sample ground for 100 minutes exhibits granular structure with

grains sizing from 100 nm to 10 μm. Sintering was much efficient when powders were previously ground for more than 150 min, as shown in SEM images.

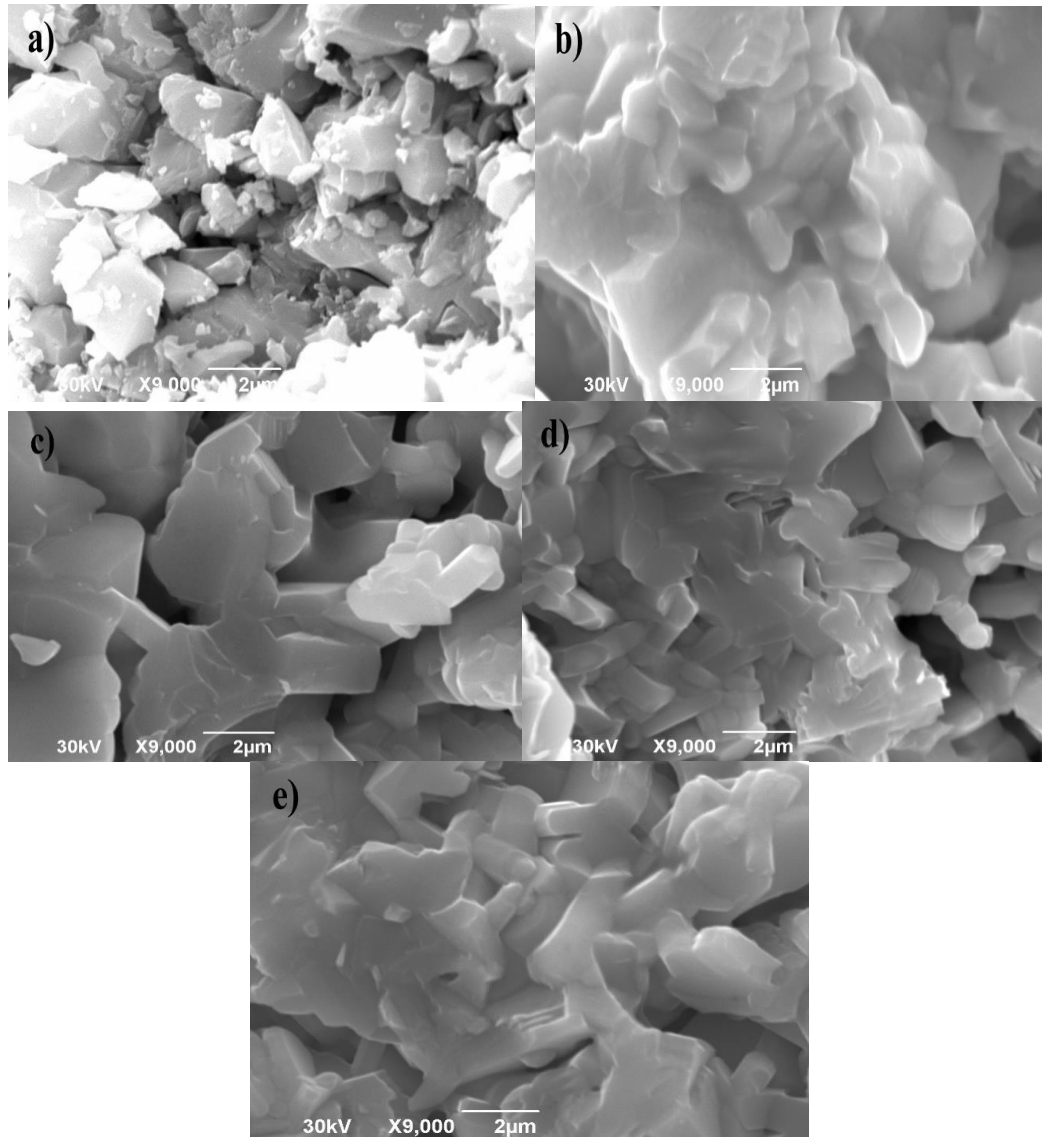


Fig. 12. SEM images of samples sintered at 1200°C and previously ground for: a) 100 min; b) 150 min; c) 180 min; d) 210 min; e) 240 min

Relatively compact, sintered samples are obtained from powders ground for 180 to 240 min. Individual grains in these samples are hardly noticeable. Mapping of the elements shows the presence of a matrix with a large density of both elements Ba and Fe. Equally distributed spots with a large density of the Ti element are found in the matrix. Therefore, the sintered samples, previously ground for 210 min and more than 210 min, are composed of the matrix

consisting of $\text{BaFe}_{12}\text{O}_{19}$ with TiO_2 stuck within. Fig. 13 shows the XRD diffractogram of the sample obtained from the powder sintered for 2h at 1200°C. The powder for sintering is obtained by grinding the initial mixture for 30 minutes. The peaks of both $\alpha\text{-Fe}_2\text{O}_3$ and $\text{BaFe}_{12}\text{O}_{19}$ are identified in the diffractograms [13]. The crystalline fraction of the powder is composed of 57,1 wt% $\text{BaFe}_{12}\text{O}_{19}$ and 42,9 wt% $\alpha\text{-Fe}_2\text{O}_3$.

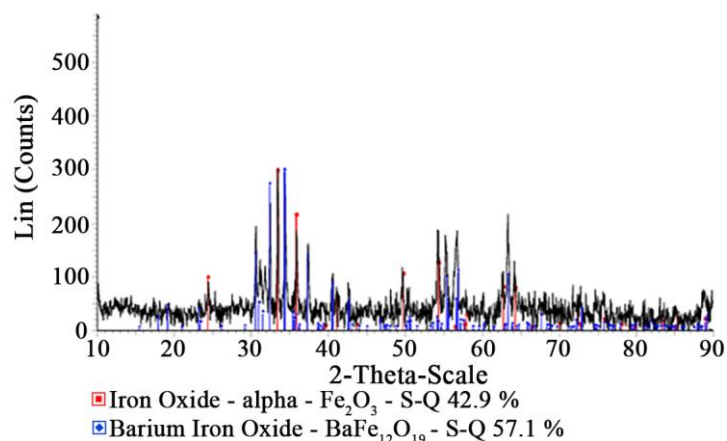


Fig. 13. XRD patterns of samples of sintered powders ground for 30 min (color online)

Grinding for 30 min results in relatively large both BaTiO₃ and Fe-containing particles. Due to relatively small contact surface between these particles, 2 h time of sintering at 1200°C is not sufficient to complete the reaction of BaFe₁₂O₁₉ formation. Well-defined peaks of titanium oxides are not observed in the diffractogram. Most probably, these oxides exist in the amorphous state since the sintering time is insufficient to form crystalline TiO₂. The increase in the grinding time results in smaller particles. A larger contact surface between smaller BaTiO₃ and Fe-containing particles allows for faster formation of BaFe₁₂O₁₉ (Fig. 14 and Fig. 15) [12, 24–26]. The most

efficient formation of the BaFe₁₂O₁₉ nanocrystals occurs in a sintered sample, obtained from the powder ground for 240 min. Diffractogram of this sample for different crystalline plates shows the highest intensities of peaks and the smallest widths of the half heights. Sintered samples, obtained from powders ground for more than 270 minutes, have lower intensity peaks. Most probably, during sintering, fast formation of nucleus of BaFe₁₂O₁₉ occurs in these powders. As a consequence, a large number of fine nanocrystals and partially, the amorphous phase of BaFe₁₂O₁₉ are formed.

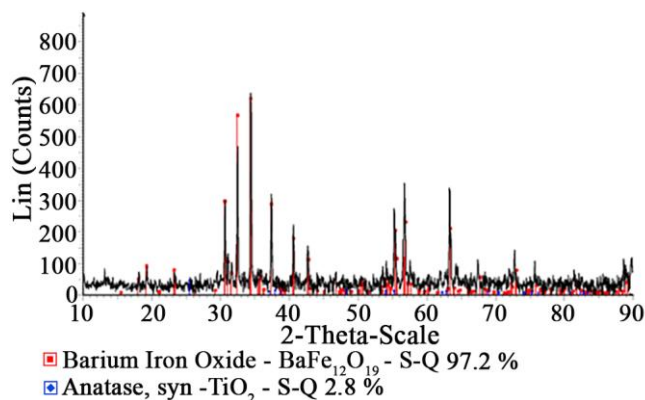


Fig. 14. XRD patterns of samples of sintered powders ground for 240 min (color online)

Weight percentages of crystalline phases of BaFe₁₂O₁₉ and Fe₂O₃ in their crystalline mixture are presented with the solid line in Fig. 15. These percentages were determined from the ratio of relative integrals of the peak intensities of a given phase from the XRD pattern to sum of relative integrals of peak intensities of both phases. The dashed line

represents the BaFe₁₂O₁₉ content reduced by formation of the amorphous phase. This content was determined from the ratio of the relative integral of peak intensities of the BaFe₁₂O₁₉ sample, obtained from the powder ground for $t > 240$ min to the relative integral of peaks of the powder sample, ground for 240 minutes.

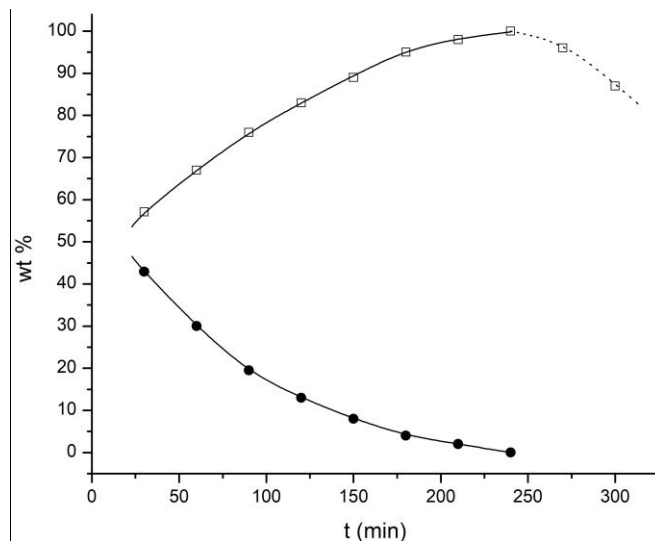


Fig. 15. Weight % of the crystalline phase ● - $\alpha\text{-Fe}_2\text{O}_3$ and □ - $\text{BaFe}_{12}\text{O}_{19}$ in their crystalline mixture of the sintered samples as a function of the grinding time. The dashed line presents reduced contents of the $\text{BaFe}_{12}\text{O}_{19}$ samples, ground for more than 240 min when compared to the contents of the samples ground for 240 min.

The roentgenogram presented in Fig. 14 shows that 97.2 wt% of the crystalline structure of the sintered sample, ground for 240 minute, derives from $\text{BaFe}_{12}\text{O}_{19}$, whereas only 2.8 wt% is from TiO_2 structure anatase. These results indicate that most of titanium oxide is in the amorphous state.

Magnetic properties of the powders are determined from a magnetization of a) pressed and b) pressed and sintered samples. The magnetization of the pressed samples as a function of the grinding time in a magnetic field of: 10 kAm^{-1} ; 30 kAm^{-1} and 40 kAm^{-1} is presented in Fig. 16.

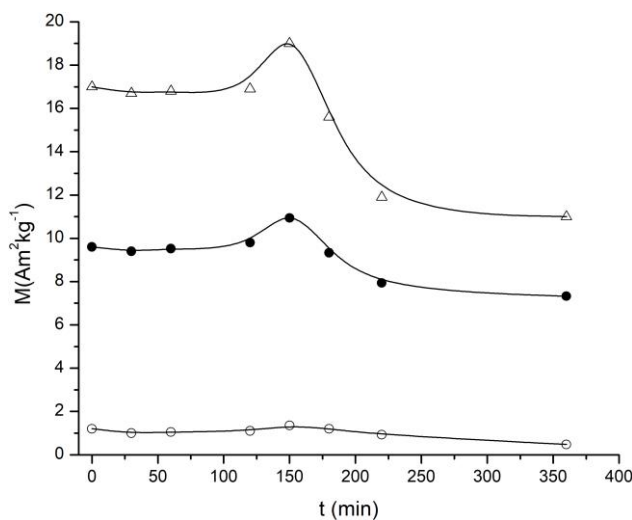


Fig. 16. Magnetization of the pressed samples as a function of the grinding time and the applied magnetic field strength: ○ - 10 kAm^{-1} ; ● - 30 kAm^{-1} and △ - 40 kAm^{-1} at 25°C

The powder ground for 150 min shows the highest magnetization in all applied magnetic fields, as seen in Fig. 16. Structural changes of the powder, caused by the grinding process, affect its magnetic properties [20–26]. Crushing of the iron crystals into smaller particles causes the increased magnetization. The increase in the density of chaotically distributed dislocations and inner microstrains declines the magnetization [20–26]. Additionally, both the decrease in the fraction of metallic iron and formation of iron oxides decline the mass magnetization. Moreover, the magnetization value depends on the composition and

structure of the mixture of iron oxides. Crushing of the iron crystals is a leading effect, causing the increase in the magnetization when the grinding time increases to 150 min. The decrease in magnetization of the sample with increasing the grinding time above 150 min is attributed to lowering of the content of metallic iron and increasing of both the density of chaotically distributed dislocations and inner microstrains [20–26].

The effect of heating on magnetic properties of pressed powders was also studied. The powders ground for 150 min were used in this examinations. The pressed sample was

heated with the heating rate of 20°C min⁻¹ to desired temperature, t_{max} and the magnetization was simultaneously determined. When maximum temperature was achieved, the sample was annealed for 10 minutes. Subsequently, the sample was cooled down to room temperature. This process was repeated five times with the same sample, in which the

sample was heated to higher temperature with each heating step.

Fig. 17 shows dependence of the magnetization of a sample on temperature. The strength of the external magnetic field was 30 kAm⁻¹.

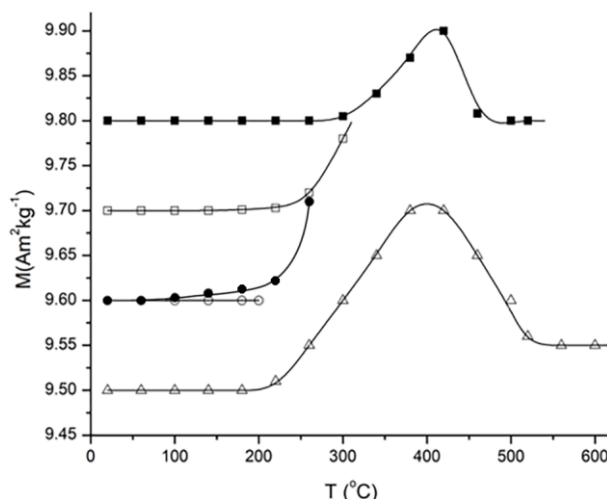


Fig. 17. Temperature dependence of magnetization of the pressed sample obtained from the powder ground for 150 min:

- - the first heating to 200°C ● - the second heating to 260°C
- - the third heating to 310°C ■ - the fourth heating to 520°C
- △ - the fifth heating to 600°C

The dependence of the magnetization of the sample cooled at 25°C on maximum temperature of previous

annealing is presented in Fig. 18. The strength of the external magnetic field was 30 kAm⁻¹.

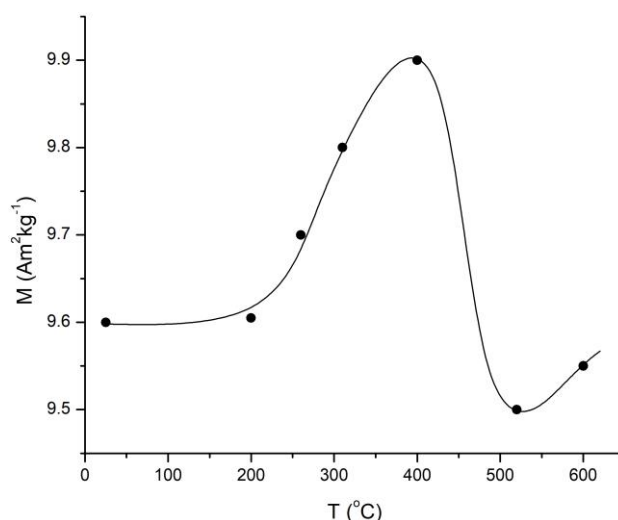


Fig. 18. Magnetization of the pressed sample of powder, ground for 150 min at 25°C as a function of maximum temperature of previous annealing

Figs. 17 and 18 show that the increased magnetization of the cooled samples results from irreversible structural changes, occurring in the sample due to annealing in the temperature range from 200 to 310°C. Similarities between roentgenograms of initial samples and those annealed at temperatures up to 310°C indicate that chemical reactions and irreversible phase transformations did not occur substantially. The increase in the magnetization during

annealing in the temperature range from 200 to 310°C is attributed to the structural relaxation [28-31]. The relaxed structure has the lower density of chaotically distributed dislocations, lower inner microstrains and lower residual stress, that allows for a) an easier orientation of individual magnetic domains, and b) a greater mobility of domain walls and thus, greater widening of the walls [26, 28-31]. By rising temperature from 310 to 400°C during the fourth

heating step, the magnetization increases. This magnetization change results from formation of the Fe_3O_4 and Fe_2O_3 nanocrystals by oxidation of amorphous oxide FeO in the presence of air oxygen. Formation of these oxides is confirmed by the XRD analysis. During the fourth heating step, with increasing temperature from 400 to 460°C, the magnetization declines. This is caused by a) the effect of the thermal energy, which reorganizes oriented magnetic domains of Fe_3O_4 nanocrystals into a chaotic state (Curie temperature of Fe_3O_4 is 585°C) and b) formation of larger nanocrystals of both Fe_3O_4 and Fe_2O_3 . During the fourth heating step in the temperature range from 460 to 520°C, the magnetization does not change substantially. In this temperature range, the magnetization predominantly

originates from domains of Fe_2O_3 nanocrystals whose Curie temperature is 675°C. During the fifth heating to 600°C, FeO and Fe_3O_4 oxidized and new additional quantities of Fe_2O_3 are formed. Therefore, the sample annealed at 600°C and then cooled to 25°C shows higher magnetization than the cooled sample, previously annealed at 520°C (Fig. 18).

Magnetic properties of sintered powders are also studied. After grinding and pressing, the obtained samples were sintered for 2 hours at 1200°C. Subsequently, the magnetization of these samples was determined. Dependence of the magnetization on the grinding time is presented in Fig. 19. The magnetic field strength was 16 kAm^{-1} .

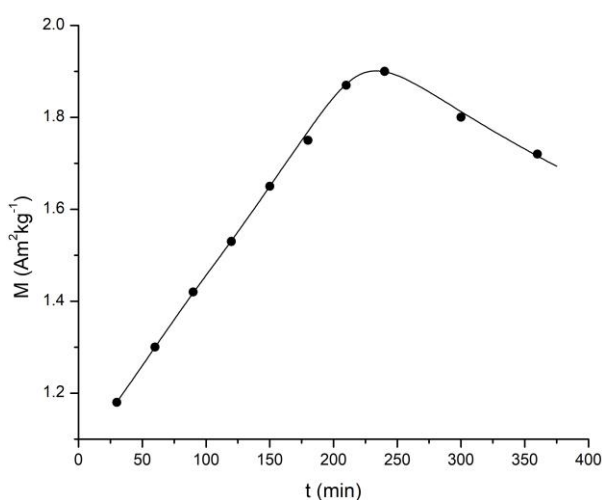


Fig. 19. Magnetization of the sintered samples at 25°C as a function of the grinding time

The sintered sample obtained from the powder ground for 240 min has the highest magnetization as shown in Fig. 19. In this sample, during sintering, entire iron, iron oxides and entire BaTiO_3 react and form $\text{BaFe}_{12}\text{O}_{19}$ and TiO_2 . By sintering the powder ground for 240 min, $\text{BaFe}_{12}\text{O}_{19}$ nanocrystals of size that provides the highest magnetization are formed. When sintering powders ground for less than 240 min, lower amounts of large $\text{BaFe}_{12}\text{O}_{19}$ nanocrystals are formed. The domains composed of large nanocrystals have lower magnetization than domains with smaller nanocrystals.

The sintered samples of powders ground for more than 240 min show lower magnetization due to the elevated fraction of the $\text{BaFe}_{12}\text{O}_{19}$ amorphous phase, and the increased density of chaotically distributed dislocations, inner microstrains and residual stress.

In order to investigate an effect of heating on magnetic properties of the sintered samples, the sample, obtained by pressing the powder ground for 240 min, is used in further studies. Fig. 20 shows dependence of the magnetization on temperature of heating. During the first heating from 25°C to the Curie temperature, $T_k = 440^\circ\text{C}$, the magnetization does not change substantially till 380°C. In the temperature range from 380°C do 440°C the orientation of magnetic domains is lost due to the effect of the thermal energy,

which further causes a decrease in the magnetization. After cooling the sample to 25°C, in the absence of the external magnetic field, its magnetization is 13% higher than the magnetization of the initial sample. The sample sintered at 1200°C cools down relatively quickly to room temperature. The process of the structural relaxation in the sample is not completed during quick cooling in the short time interval. During heating and annealing for 10 min at Curie temperature, the structural relaxation occurs in the sample. The relaxed sample contains less defects, inner microstrains and residual stress, and its magnetic domains are easily oriented in the external magnetic field. During the second heating to the Curie temperature, the effect of temperature on the magnetization is similar to that of the first heating. Specifically, during the second heating, as a result of the occurred structural relaxation, the magnetization is 13% higher than the value obtained after the first heating step [20, 21, 26, 28–31]. After the second heating, the sample was cooled to 25°C in the external magnetic field of $H = 16 \text{ kAm}^{-1}$. During the cooling process, the magnetization increases (Fig. 20). The obtained samples, cooled to 25°C show 196% higher magnetization than the as-sintered sample. Undoubtedly, the external magnetic field contributes to this substantial increase in the magnetization. During annealing at the Curie temperature, Fe atoms are

found at higher energy levels due to the thermal energy effect. While cooling the sample, the thermal energy is decreasing allowing for two processes to occur simultaneously. The first process refers to transition of atoms to lower energy states, whereas the second implies orientation of magnetic domains. Higher energy states of atoms facilitate the orientation of magnetic moments. During the cooling in the external magnetic field, the

orientation of magnetic domains occurs faster than the atom transition to lower energy levels. A result of difference in rates of these two processes is a continual increase in magnetization when lowering temperature to 25°C. The sample remains magnetized at 25°C even in the absence of external magnetic field. At a relatively low temperature of 25°C, the thermal energy is insufficient to reorganize magnetic moments into a chaotic state.

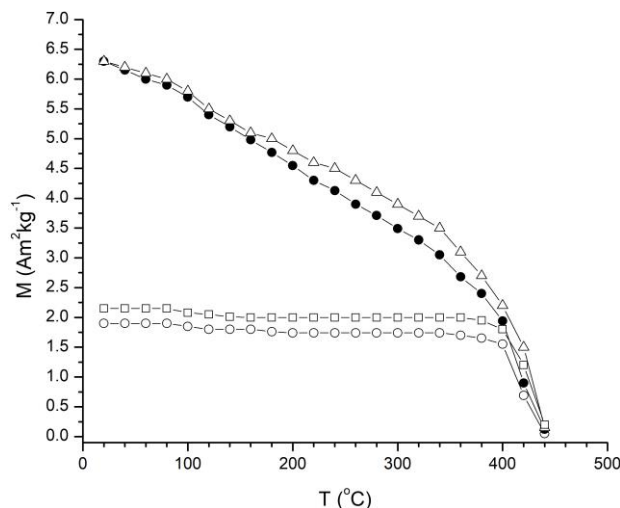


Fig. 20. Temperature dependence of the magnetization of the sintered sample, obtained from the powder ground for 240 min : \circ – the first heating; \square – the second heating (after the first cooling in the absence of magnetic field) \bullet – the second cooling and Δ – the third heating in the magnetic field of $H = 16.0 \text{ kAm}^{-1}$.

A microstructure and hence, electrical properties of a sample depend on the sample's preparation method [12, 13, 32, 33]. The grinding time of powders, used to prepare the

sintered samples, also affects the electrical properties [12, 13]. Fig. 21 shows the real and imaginary dielectric permittivity as a function of the grinding time.

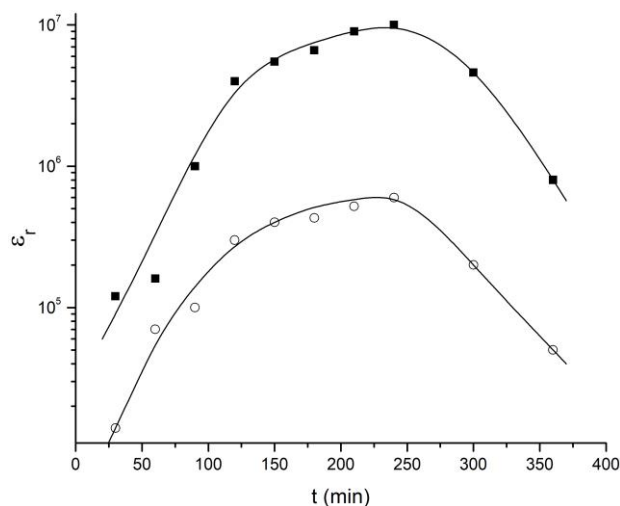


Fig. 21. The \circ – real and \blacksquare – imaginary dielectric permittivity of the sintered sample as a function of the grinding time of the powder. The frequency of the applied voltage is 50 Hz.

With increasing the grinding time from 30 to 240 minutes, both real and imaginary parts of the dielectric permittivity increase and reach the maximum in 240 minutes, as shown in Fig. 21. Further increase in the grinding time above 240 minutes results in the decrease of

the permittivity. The increase in the permittivity with increasing the grinding time from 30 to 240 minutes is a result of: a) the increase in the content of BaFe₁₂O₁₉ and b) the decrease in the size of nanocrystals of the tested samples. The permittivity of samples ground for more than

240 minutes decreases with increasing the grinding time due to: a) the decrease in the content of the $\text{BaFe}_{12}\text{O}_{19}$ nanocrystalline phase and b) the increase in inner microstrains, defects and residual stress in the $\text{BaFe}_{12}\text{O}_{19}$ crystals.

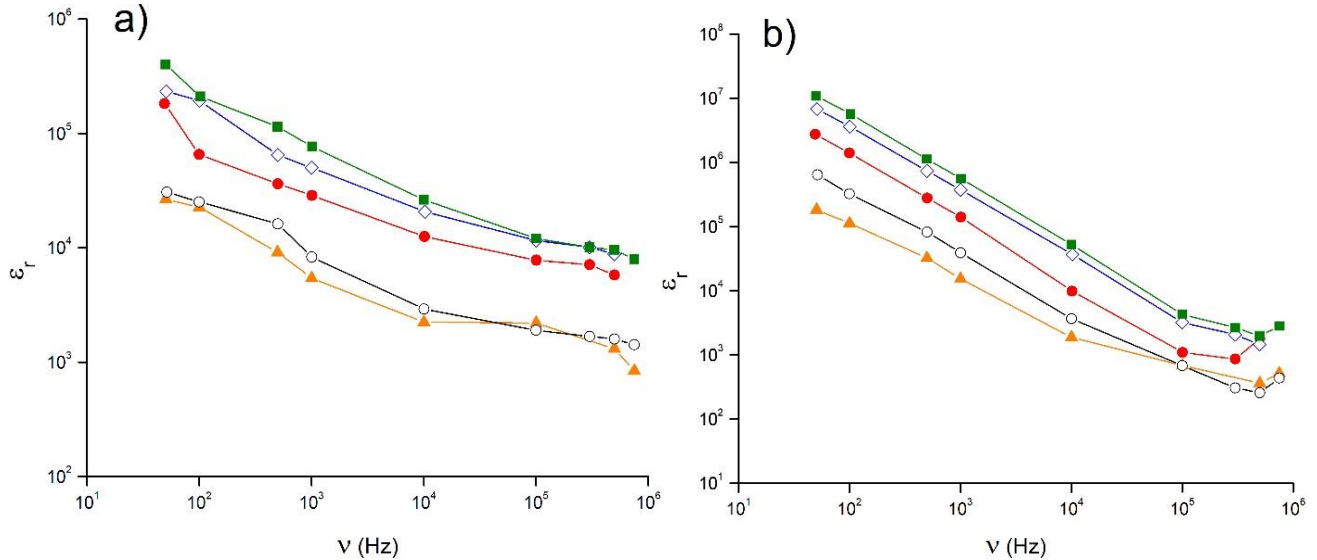


Fig. 22. a) The real and b) imaginary dielectric permittivity as a function of frequency. Sintered samples obtained from powders ground for ▲ - 30 min; ● - 120 min; ◇ - 210 min; ■ - 240 min and ○ - 300 min (color online)

Diagrams in Fig. 22 show a decrease in both real and imaginary permittivity with an increase in the frequency [12, 33]. For example, the increase in the frequency from $6 \cdot 10^1$ to 10^6 Hz results in the decrease in the real permittivity of the sample ground for 240 minutes from $1.4 \cdot 10^5$ to $8.5 \cdot 10^3$.

The dependence of the real and imaginary dielectric permittivity on temperature of the sintered sample obtained from the powder ground for 240 minutes is shown in Fig. 23.

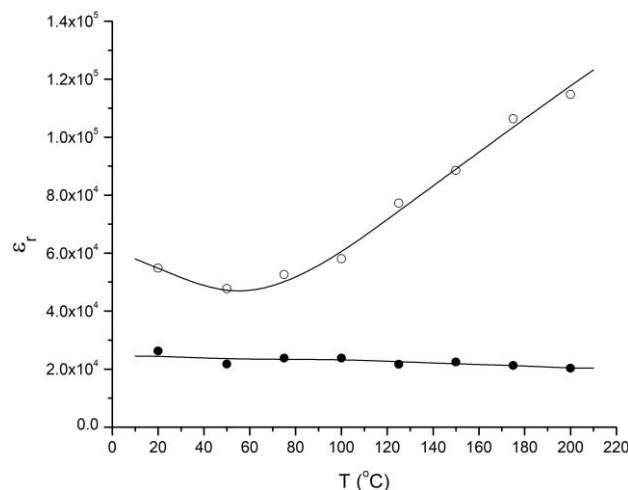


Fig. 23. Temperature dependence of the ● - real and ○ - imaginary dielectric permittivity of the sintered sample obtained from the powder ground for 240 minutes, at a frequency of $\nu = 10$ kHz

The real permittivity is stable in the temperature range from 20 to 200°C , whereas the imaginary permittivity stays steady when heated from 20 to 90°C , as seen in Fig. 23. The imaginary permittivity increases from $5.5 \cdot 10^4$ to $11.7 \cdot 10^4$ with increasing temperature from 90 to 200°C .

The decrease in the dielectric permittivity with increasing the frequency can be explained by the existence of interfacial polarization based on the two-layer model [32, 34]. High values of the dielectric permittivity at low frequencies can be attributed to a double-layer charge polarization produced at the grain boundaries. At higher

frequencies, the electron transfer between Fe²⁺ and Fe³⁺ ions occurs at the frequency lower than that of the external field, causing dispersion [13, 33, 35].

4. Conclusions

The mixture of powders consisting of 70 wt% Fe and 30 wt% BaTiO₃ is ground in a planetary mill for different periods of time. XRD, EDS and SEM analyses show that the composition, phase structure and morphology of the obtained mixtures depend on the grinding time. With increasing the grinding time, smaller particles of BaTiO₃ and Fe with finer nanocrystals and larger both the density of chaotically distributed dislocations and inner microstrains are obtained. During grinding, as a result of Fe oxidation oxides of mainly amorphous structure are formed. The thermal energy and mechanical force affect the surface layer of BaTiO₃ causing decomposition of a crystalline lattice and formation of an amorphous phase. Aggregates of BaTiO₃ particles and aggregates of Fe particles emerge as a result of grinding. The size and shape of these aggregates are found to be dependent on the grinding time. During grinding, modifications in the structure and morphology of the particles cause changes in magnetic properties of the mixture. The highest magnetization is found in the mixture obtained by grinding the powder for 150 minutes. The powders ground for shorter time periods show lower magnetization due to larger crystalline grains. When ground for more than 150 minutes, the powders also exhibit lower magnetization as a result of a lower content of metallic Fe, a higher density of chaotically distributed dislocations and larger inner microstrains in the crystalline grains.

The structural relaxation occurs in the powder, ground for 150 minutes, when annealing in the temperature range from 200 to 310 °C. The relaxed structure has lower density of chaotically distributed dislocations, inner microstrains and residual stress, and thus, the higher magnetization.

The grinding time considerably affects the efficiency of sintering. Sintering at 1200°C results in formation of both BaFe₁₂O₁₉ and TiO₂ in the powder. The most efficient sintering is achieved with powders ground for 180 to 270 minutes. Those sintered samples are compact with no individual grains observed. Formation of BaFe₁₂O₁₉ is completed in these samples. The sintered samples, obtained from powders ground for less than 180 minutes, exhibit a granular structure. In these samples formation of BaFe₁₂O₁₉ is uncompleted.

The grinding time affects the magnetization of sintered samples of pressed powders. The highest magnetization is found in the samples obtained from powders ground for 240 minutes. During sintering, the maximum amount of crystalline BaFe₁₂O₁₉ with the optimal crystal size is formed in these samples. Lower amounts of BaFe₁₂O₁₉ with larger nanocrystals, which form domains with lower magnetization, are obtained by sintering the samples obtained from ground and pressed powders, ground for less than 240 minutes. The samples, sintered from powders ground for more than 240 minutes have a larger fraction of the BaFe₁₂O₁₉ amorphous phase and the higher density of chaotically distributed dislocations, inner microstrains and

residual stress. Therefore, their magnetization is lower. Annealing of the sintered samples at the Curie temperature causes the structural relaxation of these samples. After this structural relaxation, the cooled samples show 1.96 times higher magnetization. However, after annealing at the Curie temperature and subsequent cooling to 25° in the external magnetic field, the cooled sample shows 196% higher magnetization than the as-sintered sample.

The grinding time of powders affects the electric permittivity of the sintered samples. With increasing the grinding time to 240 minutes, both the real and imaginary parts of dielectric permittivity increase. This is a result of the increase in the BaFe₁₂O₁₉ content. The dielectric permittivity declines with further increase in the grinding time above 240 minutes. This is a consequence of the decrease in the BaFe₁₂O₁₉ crystalline phase content and the increase in the density of chaotically distributed dislocations, inner microstrains and residual stress.

Acknowledgments

This study was financially supported by the Ministry of Education and Science of the Republic of Serbia through Project Ref. No. 170257.

References

- [1] R. C. Pullar, *Prog Mater Sci* **57**, 1191 (2012).
- [2] G. Y. C (1992) Concise encyclopedia of magnetic and superconducting materials, (ed.) Jan Evetts. Pergamon Press, Oxford, 1992.
- [3] K. F. Wang, J. M. Liu, Z. F. Ren, *Adv. Phys.* **58**, 321 (2009).
- [4] C. W. Nan, M. I. Bichurin, S. Dong, D. Viehland, G. Srinivasan, *J. Appl. Phys.* **103**, 031101 (2008).
- [5] J. F. Scott, *Nat. Mater.* **6**, 256 (2007).
- [6] K. S. Martirosyan, E. Galstyan, S. M. Hossain, Y. J. Wang, D. Litvinov, *Mater. Sci. Eng. B Solid-State Mater. Adv. Technol.* **176**, 8 (2011).
- [7] M. Radwan, M. M. Rashad, M. M. Hessien, *J. Mater. Process Technol* **181**, 106 (2007).
- [8] V. V. Soman, V. M. Nanoti, D. K. Kulkarni, *Ceram. Int.* **39**, 5713 (2013).
- [9] V. Pillai, P. Kumar, D. O. Shah, *J. Magn. Magn. Mater.* **116**, L299 (1992)
- [10] L. Junlian, Z. Yanwei, G. Cuijing, Z. Wei, Y. Xiaowei, *J. Eur. Ceram. Soc.* **30**, 993 (2010).
- [11] M. M. Rashad, M. Radwan, M. M. Hessien, *J. Alloys Compd.* **453**, 304 (2008).
- [12] W. S. Castro, R. R. Corrêa, P. I. P. Filho, J. M. R. Mercury, A. A. Cabral, *Ceram. Int.* **41**, 241 (2015).
- [13] D. Kosanović, V. A. Blagojević, A. Maričić, S. Aleksić, V. P. Pavlović, V. B. Pavlović, B. Vlahović, *Ceram. Int.* **44**, 6666 (2018).
- [14] P. Shepherd, K. K. Mallick, R. J. Green, *J. Magn. Magn. Mater.* **311**, 683 (2007).
- [15] S. Jan, *Ferrites: Physical Properties of Ferrimagnetic Oxides in Relation to Their Technical Applications*, Wiley, 1959.

- [16] S. Rajan, P. M. M. Gazzali, G. Chandrasekaran, *J. Alloys Compd.* **656**, 98 (2016).
- [17] A. Rani, J. Kolte, S. S. Vadla, P. Gopalan, *Ceram. Int.* **42**, 8010 (2016).
- [18] K. C. Verma, V. Gupta, J. Kaur, R. K. Kotnala, *J. Alloys Compd.* **578**, 5 (2013).
- [19] K. Samuvel, K. Ramachandran, *Optik* **127**, 1781 (2016).
- [20] X. Zhang, Z. Yue, Y. Zhang, *Ceram. Int.* **43**, 8611 (2017).
- [21] Z. Ristanović, A. Kalezić-Glišović, N. Mitrović, S. Đukić, D. Kosanović, A. Maričić, *Sci. Sinter.* **47**, 3 (2015).
- [22] D. Kosanović, N. Obradović, V. P. Pavlović, S. Marković, A. Maričić, G. Rasić, B. Vlahović, V. B. Pavlović, M. M. Ristić, *Mater. Sci. Eng. B Solid-State Mater. Adv. Technol.* **212**, 89 (2016).
- [23] F. M. Silva Júnior, C. W. A. Paschoal, *J. Appl. Phys.* **116**, 244110 (2014).
- [24] C. Suryanarayana, E. Ivanov, V. V. Boldyrev, *Mater. Sci. Eng. A* **304-306**, 151 (2001).
- [25] R. Arbain, M. Othman, S. Palaniandy, *Miner. Eng.* **24**, 1 (2011).
- [26] S. Bid, S. K. Pradhan, *Mater. Chem. Phys.* **82**, 27 (2003).
- [27] G. B. Harris, *Dublin Philos. Mag. J. Sci* **43**, 113 (1952).
- [28] L. Ribic-Zelenovic, M. Spasojevic, A. Maricic, M. M. Ristic, *Sci. Sinter.* **41**, 175 (2009).
- [29] N. Čirović, P. Spasojević, L. Ribić-Zelenović, P. Mašković, M. Spasojević, *Sci. Sinter.* **47**, 347 (2015).
- [30] N. Čirović, P. Spasojević, L. Ribić-Zelenović, P. Mašković, A. Maričić, M. Spasojević, *Sci. Sinter.* **48**, 1 (2016).
- [31] M. Spasojević, N. Čirović, L. Ribić-Zelenović, P. Spasojević, A. Maričić, *AJ Electrochem. Soc.* **161**, D463 (2014).
- [32] K. W. Wagner, *Ann. Phys.* **345**, 817 (1913).
- [33] R. R. Corrêa, *Caracterização elétrica, dielétrica e magnética da Hexafer-rita de Bário obtida por Moagem de Alta Energia (Thesis)*, Universidade Federal de São Carlos, São Carlos, SP (2005).
- [34] S. A. Lokare, D. R. Patil, R. S. Devan, S. S. Chougule, Y. D. Kolekar, B. K. Chougule, *Mater. Res. Bull.* **43**, 326 (2008).
- [35] C. G. Koops, *Phys. Rev.* **83**, 121 (1951).

*Corresponding author: smilica84@gmail.com